Investigation on the electromagnetic absorption properties of Ni@TiO_2 and Ni@SiO_2 composite microspheres with core-shell structure

Biao Zhao [a], Gang Shao [a, *], Bingbing Fan [a], Wanyu Zhao [a], Rui Zhang [a, b, *]

Received (in XXX, XXX) Xth XXXXXXXXX 20XX, Accepted Xth XXXXXXXXX 20XX
DOI: 10.1039/b000000x

ABSTRACT: In this work, amorphous TiO_2 and SiO_2-coated Ni composite microspheres were successfully prepared by a two-step method. The phase purity, morphology, and structure of composite microspheres are characterized by X-ray diffraction (XRD), field emission scanning electron microscopy (FESEM), energy dispersive X-ray spectroscopy (EDS), thermalgravimetric analysis (TGA), and transmission electron microscopy (TEM). Due to the presence of the insulator SiO_2 shell, the core-shell Ni/SiO_2 exhibits better antioxidation capability than that of pure Ni microspheres. The core-shell Ni/SiO_2 composite microspheres show the best microwave absorption properties than those of pure Ni microspheres and Ni/TiO_2 composites. For Ni/SiO_2 composite microspheres, an optimal reflection loss (RL) as low as −40.0 dB (99.99% absorption) was observed at 12.6 GHz with only absorber thickness of 1.5 mm. The effective absorption (below -10 dB, 90% microwave absorption) bandwidth can be adjusted between 3.1 GHz and 14.4 GHz by tuning absorber thickness in 1.5−4.5 mm. The excellent microwave absorption abilities of Ni/SiO_2 composite microspheres are attributed to higher attenuation constant, Debye relaxation, interface polarization of core-shell structure and synergetic effect between high dielectric loss and high magnetic loss.

1. Introduction

In recent years, with the fast development of modern communication science and technology, electromagnetic interference (EMI) pollution arising from the rapidly expanding business of communication devices, such as mobile phones, digital computers, radar systems and electronic household appliance has become a concerning problem. [1-3] These electromagnetic waves can harm the human body and can also affect the life and performance of electrical circuits. [4, 5] Consequently, there is a high demand for absorbing materials, which can absorb microwaves effectively and convert EM energy into thermal energy. [6, 7] Ideal EM absorption material should meet the following demands: thin thickness, light weight, wide absorption band, and strong absorption. [8-10]

As a candidate for microwave absorption, nickel has been extensively studied for the area of microwave absorption due to its high permeability at GHz frequency ranges, easy preparation, as well as low cost. [11-15] Nevertheless, Ni would generate eddy current induced by microwave in GHz range because of high conductivity. The eddy current could lead to impedance mismatching between the materials and air space, which would increase microwave reflection and decrease microwave absorption. This problem is a challenge to many researchers. Therefore, in order to optimize microwave absorption ability, an efficient strategy is to cover the magnetic Ni particles by an inorganic and nonmagnetic coating to create a core/shell microstructure. Extensive studies have been conducted on the uniform coating of the metal Ni with inorganic and nonmagnetic shells. For example, Ni/SnO_2 core-shell composite, [16] carbon-coated Ni,[17] Ni/ZnO ,[18] Al/AlOx-coated Ni, [19] Ni@Ni_2O_3 core–shell particles, [20] Ni/polyaniline, [21] and CuO/Cu_2O-coated Ni [22] show the better microwave absorption performance than the pure core or shell materials. Thus, the electromagnetic wave absorption abilities of Ni particles can be obviously enhanced after coating inorganic and nonmagnetic shells.

Titanium oxide (TiO_2) is an important semiconductor which holds thermally stable properties and high relative dielectric constant, so it can be used for potential microwave absorption. [23, 24] Liu and co-workers have reported Fe_3O_4@TiO_2 core–shell microspheres exhibit a much lower reflection loss and wider absorption frequency range than pure Fe_3O_4. [25] Chen and co-workers have successfully prepared Fe_3O_4/TiO_2 core/shell nanotubes with excellent microwave attenuation properties. [26] Silicon dioxide (SiO_2) often acts as a composite coating material since it is a good insulator. There are reports that the electromagnetic wave absorption properties were improved by a mixture of silicon dioxide particles. [27-30] A mixture of SiO_2 powder with a magnetic material was used to reduce the high-permeability dielectric constant and obtain good impedance match. [31]

To the best of our knowledge, there are scarce reports on the preparation and microwave absorption properties of core-shell Ni/TiO_2 and Ni/SiO_2 composites. [32] Hence, our manuscript presents a competitive work. In this work, the core-shell Ni/TiO_2 and Ni/SiO_2 composites were synthesized by a two-step process. The microwave absorption of these two core-shell composites were investigated and first compared in the frequency of 2-18 GHz. The results show the Ni/SiO_2 sample holds the strongest microwave absorption capabilities in comparison with pristine Ni and Ni/TiO_2 samples. Moreover, after coating with SiO_2 and TiO_2 shells, the EM absorption properties of Ni microspheres can be significantly enhanced.

2. Experimental section

2.1. Materials. Nickel chloride hexahydrate ($NiCl_2·6H_2O$), 1,2-propanediol, sodium acetate and trisodium citrate were purchased from Xilong Chemical Reagent Co., Ltd (China). Tetrabutyl orthotitanate (TBOT), tetraethyl orthosilicate (TEOS), ethanol, hydrazine hydrate and ammonia solution (28 wt %) were purchased from Tianjin Kaitong Chemical Reagent Co., Ltd (China). All chemicals were of analytical grade and used without further purification.

2.2. Preparation of Ni microspheres. The Ni microspheres were prepared by a solvothermal method as described previously [16]. Briefly, $NiCl_2·6H_2O$ (1.2 g, 5.0 mmol), trisodium citrate (0.3 g) and sodium acetate (3.0 g) were first dissolved in 1,2-propanediol (60 mL). Then 6 mL hydrazine hydrate was added under stirring. After that, the mixture was stirred vigorously for 30 min and then transferred into a Teflon-lined stainless-steel autoclave. The autoclave was heated at 140°C and maintained for 15 h and then allowed to cool to room temperature. Finally, the black precipitates were washed with distilled water and ethanol for several times and dried at 60°C for 10 h in a vacuum.

2.3. Synthesis of Ni@TiO_2 core−shell microspheres. The core/shell Ni/TiO_2 microspheres were synthesized via a templating approach. The as-prepared Ni microspheres (0.05 g) were dispersed in1,2-propanediol (50 mL), followed by the addition of $NH_3·H_2O$ (2 mL). Tetrabutyl orthotitanate (TBOT, 2 mL) was then added to the solution. The mixture was then transferred into a Teflon-lined stainless steel autoclave and kept at 200 °C for 15 h. After that, the products were washed with distilled water and ethanol, and dried at 60 °C in a vacuum overnight.

2.4. Synthesis of Ni@SiO_2 core−shell microspheres.

The Ni@SiO_2 microspheres were synthesized through a modified Stöber method. Typically, as-prepared Ni microspheres (0.2 g) were dispersed in a mixture of ethanol (120 mL), water (30 mL), and ammonia solution (6 mL). Afterward, 5.3 mL of TEOS was added dropwise, and the reaction was allowed to proceed for 8 h under stirring at room temperature. The final products Ni@SiO_2 microspheres were washed with distilled water and ethanol for five times and dried at 60°C for 10 h in a vacuum.

2.5. Characterization. The crystal structure of the samples were determined by X-ray diffraction (XRD, XD-3, Beijing Purkinje General Instrument Co. Ltd. Cu Kα radiation source, λ=0.15406 nm). The morphology, size and chemical composition of the synthesized samples were characterized by field-emission scanning electron microscopy equipped with energy dispersive X-ray spectroscopy (FESEM/EDS; JSM-7001F) and transmission electron microscope (TEM, FEI Tecnai 12). The composite samples used for electromagnetic measurements were prepared by mixing the products and paraffin in a mass ratio of 7:3. The mixtures were then pressed into toroidal shaped samples with an outer diameter of 7.00 mm and inner diameter of 3.04 mm. The complex permittivity and permeability of the composites were measured in the 2−18 GHz range with a vector network analyzer (Agilent N5244A).

3. Results and discussion

The synthetic strategy used for the preparation of Ni/TiO_2 and Ni/SiO_2 composites in this study is schematically illustrated in Fig.1. Firstly, uniform Ni particles were synthesized by a solvothermal reaction. Then the core-shell structured Ni/TiO_2 composite microspheres were prepared through a templating deposition method using TBOT as a precursor. The Ni microspheres were coated with silica layer via the versatile sol−gel process using TEOS as a precursor.

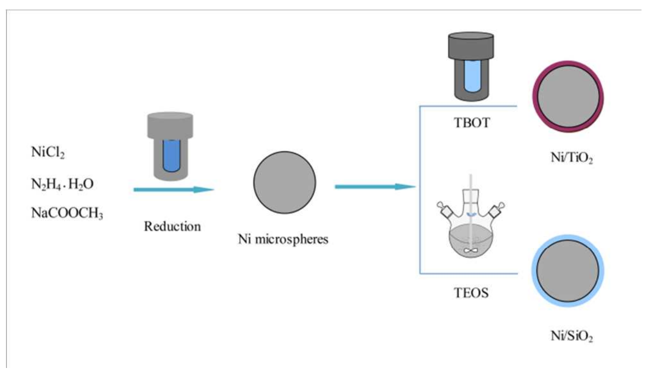

Fig.1 Schematic illustration of the formation process of the Ni/TiO_2 and Ni/SiO_2 core-shell microspheres.

To investigate the crystal structure of the products, Ni microspheres and core-shell structured composites were characterized by means of powder XRD. As shown in Fig.2a, the diffraction peaks of all samples can be well assigned to face-centred cubic (fcc) nickel ((JCPDS 04-0850). No other diffraction peaks can be detected. Notably, there is no evidence for the presence of crystalline TiO_2 and SiO_2 in the XRD patterns, which indicates that the TiO_2 and SiO_2 existing in the core-shell composites are in amorphous states. To understand the morphology of the as-prepared products, SEM measurements were carried out. Fig.2b shows the FESEM image of the Ni particles, which possess uniformly spherical shape and the diameter is about 0.8-1.0 μm. Fig. 2c shows the FESEM images of Ni/TiO_2 composites. It can be seen that all the Ni microspheres were densely coated by amorphous TiO_2. Moreover, besides the core-shell Ni/TiO_2 products existed, some irregular TiO_2 particles were also gained. From the Fig.2d, one can see that the surfaces of Ni/SiO_2 composites were rougher than Ni microspheres (Fig.2b). The Ni microspheres were covered by SiO_2 particles through sol−gel process. Based on the SEM observation, we can deduce that the core-shell structured Ni/TiO_2 and Ni/SiO_2 composites were formed through template deposition method and sol−gel process, respectively.

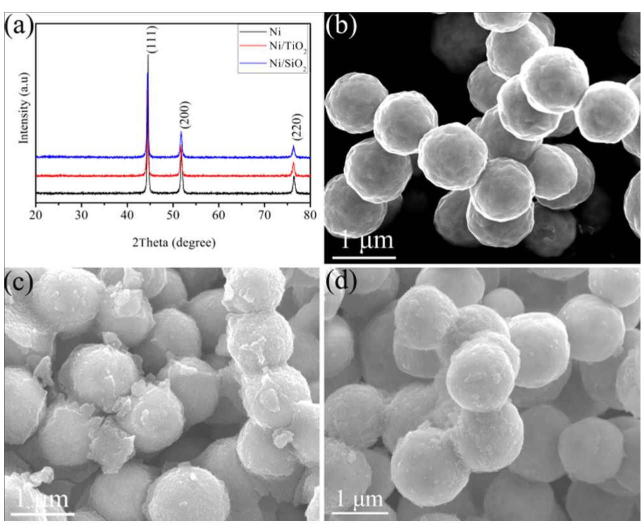

Fig.2 (a) XRD patterns of Ni, Ni/TiO_2 and Ni/SiO_2 samples. FESEM images of (b) Ni microspheres, (c) Ni/TiO_2 composites and (d) Ni/SiO_2 composites.

In order to validate the core-shell structure of Ni/TiO_2, the enlarged magnification FESEM image and EDS profile of an individual Ni/TiO_2 composite microspheres were presented in Fig.3 (a,b). It can be clearly observed that the smooth surfaces of Ni microsphere turn coarser and crinkled after coating TiO_2 shells (Fig.3a). EDS pattern of Ni/TiO_2 composite microspheres indicates that the obtained composite are composed of Ni, Ti and O elements. The C element signal originates from the carbon conductive tape to support the samples during the test. The elemental mappings of Ni/TiO_2 were also performed in Fig. 3c-e. The Ni element can be clearly detected in the core region, while the Ti element and O element can be detected in the shell regions. This further confirms the unique core-shell structures with Ni cores and TiO_2 shells.

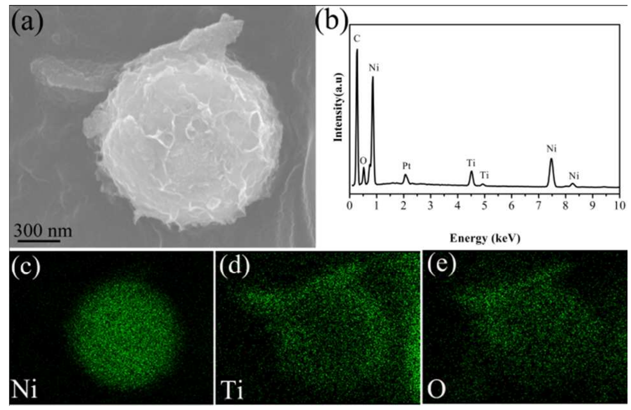

Fig.3 (a) FESEM images of an individual Ni/TiO_2 composite microsphere, (b) EDS pattern of Ni/TiO_2 composites, (c-e) elemental mappings of Ni, Ti and O.

The EDS profile and elemental mappings of an individual Ni/SiO_2 composite microsphere were also conducted in Fig.4. The EDS spectrum shown in the Fig.4b indicates the presence of three elements of Ni, Si and O in the Ni/SiO_2 product. The elemental mappings of Ni/SiO_2 were performed in Fig.4c-e. The Ni element can be clearly observed in the core region, while the Al element and O element can be detected in the shell regions. This further validates the core-shell structure of Ni/SiO_2 composite.

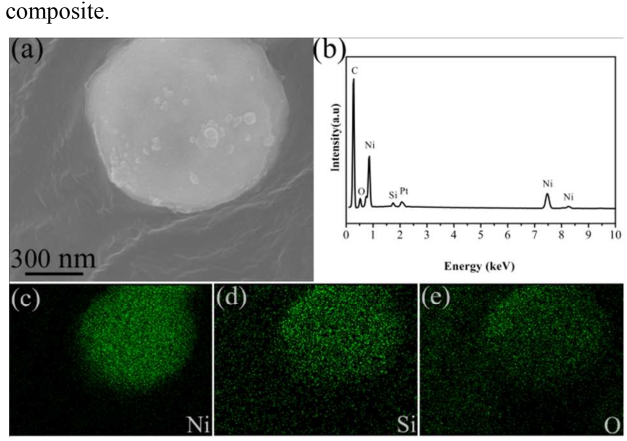

Fig.4 (a) FESEM images of an individual Ni/SiO_2 composite microsphere, (b) EDS pattern of Ni/TiO_2 composites, (c-e) elemental mappings of Ni, Si and O.

Furthermore, the TEM images are used to characterize the morphologies of Ni/TiO_2 and Ni/SiO_2 composites in detail. As shown in Fig. 5, it is clear that the Ni microspheres are fully coated by amorphous TiO_2 (Fig.5a) and SiO_2 (Fig.5b) to form core-shell structures, respectively. The thickness of shells are about dozens of nanometer. Based on the EDS, SEM and TEM results, the TiO_2 and SiO_2 were deposited on the surfaces of Ni microspheres, the core-shell composite microspheres are obtained.

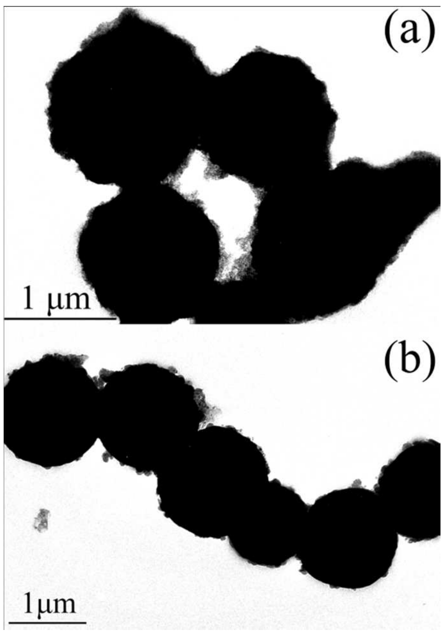

Fig.5 TEM images of (a) Ni/TiO_2 and (b) Ni/SiO_2 composites.

Fig.6 shows the electromagnetic parameters of the paraffin based composites containing 70 wt% Ni/TiO_2 and Ni/SiO_2 microspheres. It is well known that complex permittivity ($\varepsilon_r = \varepsilon' - j\varepsilon''$) and permeability ($\mu_r = \mu' - j\mu''$) paraffin-based composites are fundamental physical quantities for determining the microwave properties. [33] As shown in Fig. 6a, the real part (ε') of Ni/SiO_2 exhibits higher than that of Ni/TiO_2. In the core-shell structured products, a thin TiO_2 and SiO_2 form on the surface of the Ni particles. The TiO_2 and SiO_2 layer can introduce not only additional interfacial polarization, but also dipole polarization, contributing to the high permittivity with frequency. [34] Otherwise, the SiO_2 is insulator and TiO_2 is semiconductor. Under the microwave field, the SiO_2 shell are prone to forming more space charge on the surfaces between Ni microspheres and insulator SiO_2 shells, [35] which results in a higher real permittivity (ε'). The imaginary permittivity (ε'') is connected with the dielectric loss. [36] Fig.6b shows the imaginary parts (ε'') of Ni/TiO_2 and Ni/SiO_2 composite microspheres. It can be observed that the values of ε'' increase with the increasing frequency. Notably, the ε'' values of Ni/SiO_2 show higher than those of Ni/TiO_2. According to free-electron theory, [18] $\varepsilon'' \approx 1/\pi\varepsilon_0\rho f$, where ρ is the resistivity, the high ε'' implies the low resistivity. It indicates that the Ni/SiO_2 composite possess higher conductivity compared with Ni/TiO_2. In general, a proper high electrical conductivity is favorable for improving the microwave absorption abilities. [37]

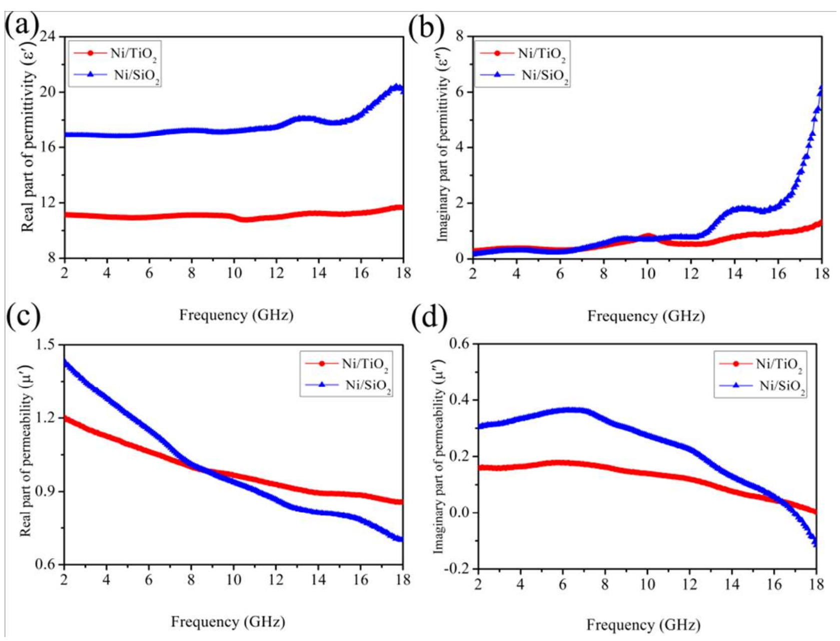

Fig.6 Frequency dependence of (a) real part and (b) imaginary parts of the relative complex permittivity, (c) real part and (d) imaginary parts of the relative complex permeability for the core-shell Ni/TiO_2 and Ni/SiO_2 composite microspheres.

The real parts (μ') of the relative complex permeability for the core-shell Ni/TiO_2 and Ni/SiO_2 composite microspheres are in the range of 0.86-1.20 and 0.70-1.43 over the frequency of 2-18 GHz, respectively (Fig.6c). The μ' values of Ni/TiO_2 and Ni/SiO_2 samples obviously decrease with increasing frequency in the 2–18 GHz range. For the μ'' values, the μ'' exhibits broad resonance peaks at 5-8 GHz, which are attributed to natural resonance of Ni. [38] It is worth noting that the μ'' of Ni/SiO_2 shows the higher values than those of Ni/TiO_2, which indicates the higher magnetic loss (Fig.6d). In addition, especially for the Ni/SiO_2 sample, the change trend of the permeability is just inverse to that of the permittivity, which attributed to the capacitance C lead or lag behind the angle of 90° than the inductance L. [39] The μ'' of Ni/SiO_2 is negative between 17 and 18 GHz. The negative μ'' value denotes that the magnetic energy is radiated out from the Ni/SiO_2 composites and transferred into the electric energy, which can greatly increase ε'' and then leads to the negative μ''. [40]

The dielectric loss tangent ($\tan \delta_\varepsilon = \varepsilon''/\varepsilon'$) and magnetic loss tangent ($\tan \delta_\mu = \mu''/\mu'$) are commonly used to describe electromagnetic loss capacity. [41] The excellent electromagnetic wave absorptions are strongly dependent on the efficient complementarities between the relative permittivity and permeability. Only magnetic loss or dielectric loss leads to weak EM attenuation. [42] Therefore, we calculate the tangent losses based on the data in Fig. 6, and the calculated results are shown in Fig. 7. Notably, for the Ni/TiO_2 and Ni/SiO_2 composites, one can see that the magnetic loss plays the crucial role in the EM absorption in the low-frequency range while magnetic loss play a vital role in the in the EM absorption at the high-frequency range. It demonstrates that the core/shell structured Ni/TiO_2 and Ni/SiO_2 samples hold good complementarities between the dielectric loss and the magnetic loss, which suggests they have excellent EM wave absorption properties. It can also be found that the Ni/SiO_2 presents higher dielectric loss than Ni/TiO_2 at low frequency and higher magnetic loss than Ni/TiO_2 at high frequency, which indicates that the Ni/SiO_2 sample possesses better microwave attenuation capabilities than Ni/TiO_2.

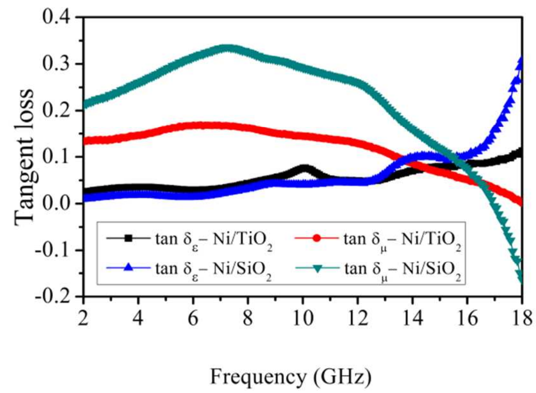

Fig.7 The dielectric loss tangent ($\tan \delta_\varepsilon = \varepsilon''/\varepsilon'$) and magnetic loss tangent ($\tan \delta_\mu = \mu''/\mu'$) of core-shell Ni/TiO_2 and Ni/SiO_2 composites as functions of frequency.

The dielectric loss is likely caused by Debye dipolar relaxation, which is a crucial mechanism for the composite to absorb microwaves.[43, 44] If the Debye relaxation process accounts for dielectric loss behavior, the relationship between ε' and ε'' can be deduced as shown in Equation:

$$(\varepsilon' - \frac{\varepsilon_s + \varepsilon_\infty}{2})^2 + (\varepsilon'')^2 = (\frac{\varepsilon_s - \varepsilon_\infty}{2})^2 \qquad (1)$$

Thus, the plot of ε' versus ε'' would be a single semicircle, generally denoted as the Cole–Cole semicircle. [45] Fig. 8b shows the ε'-ε'' curve of Ni/TiO_2 and Ni/SiO_2-wax composite. It can be observed that three semicircles were found in the Ni/SiO_2–wax composite (Fig.8b) and two semicircles for Ni/TiO_2–wax composite (Fig.8a). It is well known that the relaxation time is associate with the relaxation process. For the metal-semiconductor (Ni@TiO_2) system, the charge migration easily happen because of different electronegativity between Ni and TiO_2 under the alternating electromagnetic field. While in the metal-insulator (Ni@SiO_2), the movement of charge only occur in the Ni cores. Thus the interfacial relaxation between Ni and SiO_2 insulator become difficult and the relaxation time gets long, which induce more wave energy dissipated. However, the Cole–Cole semicircles are distorted, suggesting that besides the Debye relaxation, other mechanisms also exist in core-shell Ni/TiO_2 and Ni/SiO_2 wax-composite. Other kinds of loss mechanisms are Maxwell–Wagner relaxation and electron polarization. The former behavior appears in heterogeneous media owing to the accumulation of charges at the interfaces and the formation of large dipoles on particles or clusters. In core-shell structured composites, the existence of interfaces gives rise to interfacial polarization (Maxwell–Wagner effect). [46]

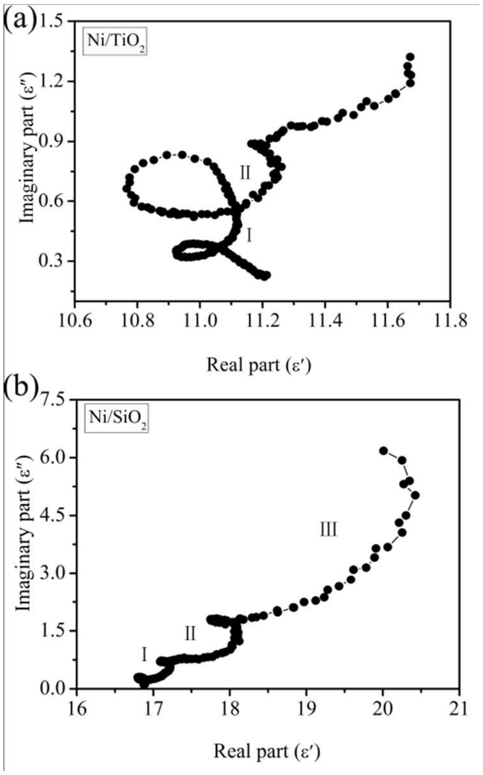

Fig.8 The relation between real part (ε′) and imaginary part (ε″) of the complex permittivity (Cole–Cole plot).

In general, the magnetic loss of magnetic materials stems from hysteresis loss, domain wall displacement loss, eddy current loss and natural resonance. In our case, the hysteresis loss is negligible in weak applied field. [47] The domain wall displacement loss occurs only in the MHz range rather than GHz, so the contribution of domain wall resonance can also be excluded. [48] The eddy current loss is correlated to the diameter (d) and the electric conductivity (σ), which can be expressed by [49] $\mu'' \approx 2\pi\mu_{\circ}(\mu')^2\sigma d^2 f/3$. In which f is the applied frequency, μ_0 is the vacuum permeability. Based on this equation, supposing that the magnetic loss only originates from eddy current loss, the values of $C_0(C_0 = \mu''(\mu')^{-2} f^{-1} = 2\pi\mu_0\sigma d^2/3)$ should be constant with varying frequency, which is called the skin-effect criterion [47]. In Ni/TiO_2 and Ni/SiO_2 composite, the value of C_0 decrease gradually with increasing frequency in the whole range of 2–18 GHz (Fig. 9). Therefore, the magnetic loss in the present samples is mainly caused by the nature resonance.

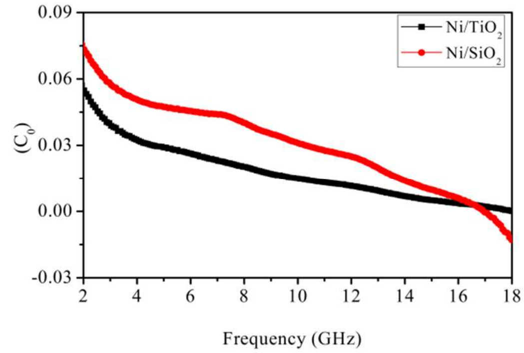

Fig.9 The value C_0 ($\mu''(\mu')^{-2} f^{-1}$) of Ni/TiO_2 and Ni/SiO_2 composite microspheres as a function of frequency.

To evaluate the electromagnetic absorption performance of the Ni/TiO_2 and Ni/SiO_2 samples, their refection loss (RL) values were calculated based on the measured complex permittivity and permeability: [50, 51]

$$RL = 20\log\left|\frac{Z_{in}-1}{Z_{in}+1}\right| \quad (2)$$

$$Z_{in} = \sqrt{\frac{\mu_r}{\varepsilon_r}}\tanh\left[j\left(\frac{2\pi fd}{c}\right)\sqrt{\mu_r\varepsilon_r}\right] \quad (3)$$

where Z_0 is the impedance of free space, Z_{in} is the input impedance of the absorber, f is the frequency of the electromagnetic waves, c is the velocity of electromagnetic waves in free space, μ_r and ε_r are, respectively, the relative complex permeability and permittivity, and d is the thickness of the absorber. Fig. 10a shows the reflection loss versus frequency for Ni/TiO_2 wax composite with the various thicknesses. The minimum reflection loss is –35.4 dB at 17.8 GHz with the thickness of 4.0 mm. However, the band of RL below -10 dB is narrow. In comparison with Ni/TiO_2 composite, the Ni/SiO_2 paraffin composite reveals better microwave absorption performance. As shown in Fig.10b, the lowest reflection loss is –40.0 dB at 12.6 GHz and RL below -10 dB is 3.5 GHz (10.9-14.4 GHz) with the only thickness of 1.5 mm.. The effective absorption (below -10 dB) bandwidth can be tuned between 3.1 GHz and 14.4 GHz for the absorber with the thin thickness in 1.5−4.5 mm. It can be found that the attenuation peaks would shift to lower frequencies and two RL peaks appear with the increasing thickness. It can be explained by the quarter-wavelength cancellation model that the incident and reflected waves in the absorber are out of phase 180°, which lead to the reflected waves in the air-absorber interface totally cancelled. [52, 53] Fig. 10c shows the bandwidth of the absorption frequency of

Ni/SiO$_2$ samples for RL< -10 dB in a two-dimensional contour plot. The result indicates that a thinner absorber layer has a wider frequency bandwidth. To probe the effect of core-shell structure on the microwave attenuation of Ni/TiO$_2$ and Ni/SiO$_2$ composite, the reflection loss of bare Ni microspheres was also investigated (Fig. 10d). It is worth noting that the microwave absorption property of the pure Ni microspheres is very weak, which indicates the microwave absorption of Ni microspheres can be obviously improved after coating with TiO$_2$ and SiO$_2$ shells. Table 1 shows the typical Ni-based composites and their corresponding microwave absorption performances in recent literatures.[11, 12 14-17, 19, 21, 38, 50, 54-57] According to the comparison, the core-shell structured Ni/SiO$_2$ composite microspheres are very promising to be used as thin-thickness, and high EM wave absorptive materials in a wide frequency range.

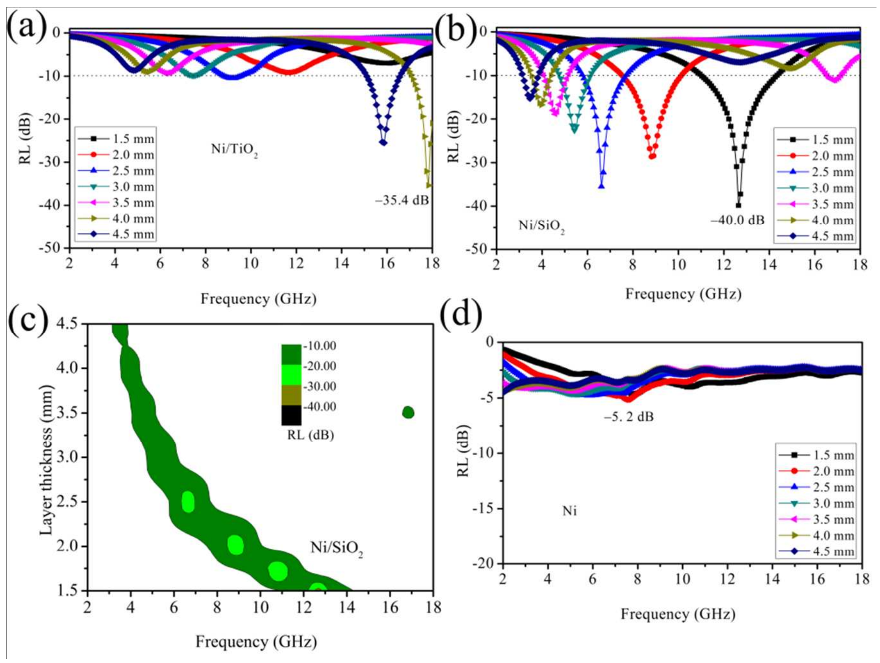

Fig.10 The reflection loss (RL) of (a) Ni/TiO$_2$, (b) Ni/SiO$_2$ and (d) pristine Ni paraffin composites with different absorber thicknesses; (b) contour map of Ni/SiO$_2$ sample (RL< −10 dB, 90% microwave absorption) as a function of the absorber thickness.

Table 1 Typical Ni-based composites for microwave absorption in recent literatures

Sample	Minimum RL Value (dB)	Optimum Thickness (mm)	Optimum Frequency (GHz)	Frequency range (RL<-10 dB)	Ref.
Octahedral Ni	–40.44	2.5	8.8	7.1–11.2	[11]
Ni fiber	–39.5	3.0	4.8	6.6–8.8	[12]
Urchin-like Ni	–43	2.0	10	8.7–11.5	[14]
Ni nanowires	–8.5	3.0	10	–	[54]
Ni conical nanorods	–37	2.5	8.0	6.7–9.5	[55]
Ni chains	–25.29	2.0	9.6	8.3–10.4	[15]
Ni/SnO$_2$	–18.6	7.0	14.7	13.8–15.3	[16]
Carbon-coated nickel	–32	2.0	13.0	11.2–15.5	[17]
Al/AlO$_x$-coated Ni	–40.96	2.4	9.2	8.2-10.8	[19]
Ni/graphene	–13	2.0	11.0	9.6–12.2	[56]
Ni/polyaniline	–35	5.0	17.2	4.9–6.1 16.2–18	[21]
Hexagonal Ni/graphene	–17.8	5.0	3.5	2.7–3.9 11.9–13.5	[38]
PS@PPy@Ni	–20.06	2.0	10.69	9.16–13.75	[50]

Ni/Polypyrrole	–15.2	2.0	13.0	11–15.4	[57]
Ni/TiO_2	–35.4	4.0	17.8	17.0–18.0	This work
Ni/SiO_2	–40.0	1.5	12.6	10.9–14.4	This work

To obtain materials with superior microwave absorption properties, there are two key problems to be solved. One is the impedance match between the material and free space, [58] which needs the permittivity is close to permeability. When the input impedance of the composite materials is closer to the wave impedance of free space, more energy of the incident microwaves can be transferred and dissipated in the absorber. In present work, SiO_2 is the most popular wave-transmitting materials, [4, 59] which makes microwave incident microwave enter into the absorber as much as possible, and largely improve the microwave absorbing properties of the samples. The other is the EM attenuation in the interior absorber. The microwave attenuation constant (α) can be expressed by:[33, 60]

$$\alpha = \frac{\sqrt{2}\pi f}{c} \times \sqrt{(\mu''\varepsilon'' - \mu'\varepsilon') + \sqrt{(\mu''\varepsilon'' - \mu'\varepsilon')^2 + (\mu'\varepsilon'' + \mu''\varepsilon')^2}} \qquad (4)$$

where f is the frequency and c is the velocity of light. Fig.11 shows the attenuation constant of Ni/TiO_2 and Ni/SiO_2 samples. The Ni/SiO_2 sample possesses bigger α in all frequency ranges, indicating the excellent attenuation or EM wave absorption. From the above equation, it is noted that high values of ε″ and μ″ would result in high α. The enhancement of the microwave absorption properties of Ni/SiO_2 sample results from the increase in dielectric loss and magnetic loss. In our present case, the Ni/SiO_2 have potential applications as superior absorbents due to the thinner thickness and higher imaginary part of the permittivity and permeability.

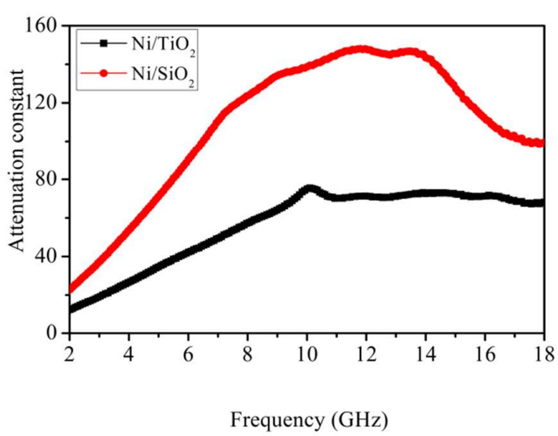

Fig.11 Attenuation constant of Ni/TiO_2 and Ni/SiO_2–paraffin composites versus frequency.

It is well known that anti-oxidant capacity is an important criterion for the application of materials. The oxidation behaviors of the pure Ni and Ni/SiO_2 are shown in **Fig.12**. The pure Ni starts to oxidize at around 270 ºC. The pristine Ni microspheres show a significant weight increase in the final stage due to the oxidation in air. After coating with a insulator SiO_2 shell, the Ni microspheres are protected, and the oxidation temperature is improved to about 505 ºC. It indicates that the core-shell Ni-SiO_2 presents better antioxidization resistance than that of Ni microsphere.

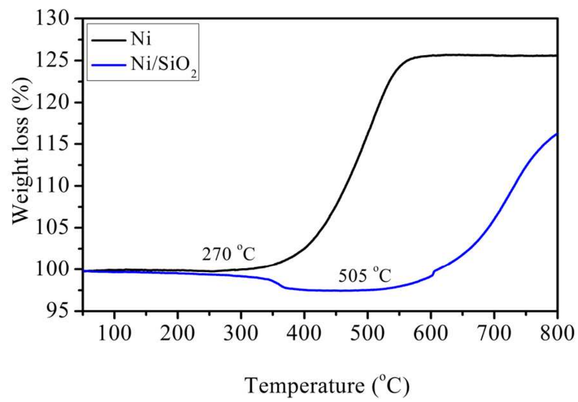

Fig.12 TG pattern of the Ni and Ni/SiO_2 composite microspheres.

4. Conclusion

In summary, the core-shell Ni/TiO_2 and Ni/SiO_2 composite microspheres have been successfully prepared by a two-step process. Compared with pristine Ni microspheres, the electromagnetic wave absorption properties of Ni/TiO_2 and Ni/SiO_2 can be significantly enhanced. The minimum reflection loss of Ni/TiO_2 is –35.4 dB at 17.8 GHz with the thickness of 4.0 mm. However, the band of RL below -10 dB is narrow. The Ni/SiO_2 paraffin composite reveals the best microwave absorption capabilities. The lowest reflection loss is –40.0 dB at 12.6 GHz and RL below -10 dB is 3.5 GHz (10.9–14.4 GHz) with the only thickness of 1.5 mm. In comparison with pristine Ni microspheres, the core-shell Ni/SiO_2 composite microspheres show better antioxidation ability. Our results reveal that the amorphous SiO_2-coated Ni core/shell composites obtained in this work with the features of high antioxidation, thin thickness, strong absorption and wideband are attractive candidates for the new types of EM wave absorptive materials.

Notes and references

[a] School of Materials Science and Engineering, Zhengzhou University, Zhengzhou, Henan 450001, PR China

[b] Zhengzhou Aeronautical Institute of Industry Management, Zhengzhou, Henan 450046, PR China

** Corresponding Author.*

Dr. Gang Shao

E-mail address: gang_shao@zzu.edu.cn

Prof. Rui Zhang

Tel: +86-371-60632007

Fax: +86-371-60632600

E-mail address: zhangray@zzu.edu.cn.

1. H. Hekmatara, M. Seifi, K. Forooraghi and S. Mirzaee, *Phys. Chem. Chem. Phys.*, 2014, **16**, 24069-24075.
2. G. Li, L. Wang, W. Li, R. Ding and Y. Xu, *Phys. Chem. Chem. Phys.*, 2014, **16**, 12385-12392.
3. C. Hu, Z. Mou, G. Lu, N. Chen, Z. Dong, M. Hu and L. Qu, *Phys. Chem. Chem. Phys.*, 2013, **15**, 13038-13043.
4. J. Zhu, S. Wei, N. Haldolaarachchige, D. P. Young and Z. Guo, *J. Phys. Chem. C*, 2011, **115**, 15304-15310.
5. L. Kong, X. Yin, Y. Zhang, X. Yuan, Q. Li, F. Ye, L. Cheng and L. Zhang, *J. Phys. Chem. C*, 2013, **117**, 19701-19711.
6. Y.-L. Ren, H.-Y. Wu, M.-M. Lu, Y.-J. Chen, C.-L. Zhu, P. Gao, M.-S. Cao, C.-Y. Li and Q.-Y. Ouyang, *ACS Appl. Mater. Interfaces*, 2012, **4**, 6436-6442.
7. S.-T. Hsiao, C.-C. M. Ma, W.-H. Liao, Y.-S. Wang, S.-M. Li, Y.-C. Huang, R.-B. Yang and W.-F. Liang, *ACS Appl. Mater. Interfaces*, 2014, **6**, 10667-10678.
8. D. Sun, Q. Zou, Y. Wang, Y. Wang, W. Jiang and F. Li, *Nanoscale*, 2014, **6**, 6557-6562.
9. J. Liu, J. Cheng, R. Che, J. Xu, M. Liu and Z. Liu, *ACS Appl. Mater. Interfaces*, 2013, **5**, 2503-2509.
10. H. R. Tantawy, D. E. Aston, J. R. Smith and J. L. Young, *ACS Appl. Mater. Interfaces*, 2013, **5**, 4648-4658.
11. G. Tong, Q. Hu, W. Wu, W. Li, H. Qian and Y. Liang, *J. Mater. Chem.*, 2012, **22**, 17494-17504.
12. C. Gong, J. Zhang, X. Zhang, L. Yu, P. Zhang, Z. Wu and Z. Zhang, *J. Phys. Chem. C*, 2010, **114**, 10101-10107.
13. B. Zhao, B. Fan, G. Shao, B. Wang, X. Pian, W. Li and R. Zhang, *Appl. Surf. Sci.*, 2014, **307**, 293-300.
14. T. Liu, P. Zhou, J. Xie and L. Deng, *J. Appl. Phys.*, 2012, **111**, 093905.
15. C. Wang, X. Han, P. Xu, J. Wang, Y. Du, X. Wang, W. Qin and T. Zhang, *J. Phys. Chem. C*, 2010, **114**, 3196-3203.
16. B. Zhao, G. Shao, B. Fan, W. Li, X. Pian and R. Zhang, *Mater. Lett.*, 2014, **121**, 118-121.
17. X. F. Zhang, X. L. Dong, H. Huang, Y. Y. Liu, W. N. Wang, X. G. Zhu, B. Lv, J. P. Lei and C. G. Lee, *Appl. Phys. Lett.*, 2006, **89**, 053115.
18. X. G. Liu, J. J. Jiang, D. Y. Geng, B. Q. Li, Z. Han, W. Liu and Z. D. Zhang, *Appl. Phys. Lett.*, 2009, **94**, 053119.
19. X. Liu, C. Feng, S. W. Or, C. Jin, F. Xiao, A. Xia, W. Li, Y. Sun and S. Zhao, *Mater. Res. Bull.*, 2013, **48**, 3887-3891.
20. B. Wang, J. Zhang, T. Wang, L. Qiao and F. Li, *J. Alloys Compd.*, 2013, **567**, 21-25.
21. X. L. Dong, X. F. Zhang, H. Huang and F. Zuo, *Appl. Phys. Lett.*, 2008, **92**, 013127.
22. X. Liu, C. Feng, S. W. Or, Y. Sun, C. Jin, W. Li and Y. Lv, *RSC Adv.*, 2013, **3**, 14590-14594.
23. A. Dey, S. De, A. De and S. De, *Nanotechnology*, 2004, **15**, 1277.
24. H.-M. Xiao, X.-M. Liu and S.-Y. Fu, *Compos. Sci. Technol.*, 2006, **66**, 2003-2008.
25. J. Liu, R. Che, H. Chen, F. Zhang, F. Xia, Q. Wu and M. Wang, *Small*, 2012, **8**, 1214-1221.
26. C.-L. Zhu, M.-L. Zhang, Y.-J. Qiao, G. Xiao, F. Zhang and Y.-J. Chen, *J. Phys. Chem. C*, 2010, **114**, 16229-16235.
27. Y. Liu, X. Yin, L. Kong, X. Liu, F. Ye, L. Zhang and L. Cheng, *Carbon*, 2013, **64**, 541-544.
28. X. J. Wei, J. T. Jiang, L. Zhen, Y. X. Gong, W. Z. Shao and C. Y. Xu, *Mater. Lett.*, 2010, **64**, 57-60.
29. X. Ni, Z. Zheng, X. Hu and X. Xiao, *J. Colloid Interface Sci.*, 2010, **341**, 18-22.
30. W. Huang , P. Zhang, W. Yan, L. Zhou and H. Xu, *J. Phys. D: Appl. Phys.*, 2012, **45**, 405001.
31. H. Pan, X. Cheng, C. Zhang, C. Gong, L. Yu, J. Zhang and Z. Zhang, *Appl. Phys. Lett.*, 2013, **102**, 012410.

32. C. Gong, X. Wang, X. Zhang, X. Zhao, H. Meng, Y. Jia, J. Zhang and Z. Zhang, *Mater. Lett.*, 2014, **121**, 81-84.
33. S. L. Wen, Y. Liu, X. C. Zhao, J. W. Cheng and H. Li, *Phys. Chem. Chem. Phys.*, 2014, **16**, 18333-18340.
34. F. Ma, Y. Qin and Y.-Z. Li, *Appl. Phys. Lett.*, 2010, **96**, 202507.
35. S. Yan, L. Zhen, C. Xu, J. Jiang and W. Shao, *J. Phys. D: Appl. Phys.*, 2010, **43**, 245003.
36. X.-J. Zhang, G.-S. Wang, W.-Q. Cao, Y.-Z. Wei, J.-F. Liang, L. Guo and M.-S. Cao, *ACS Appl. Mater. Interfaces*, 2014, **6**, 7471-7478.
37. G.-S. Wang, Y. Wu, Y.-Z. Wei, X.-J. Zhang, Y. Li, L.-D. Li, B. Wen, P.-G. Yin, L. Guo and M.-S. Cao, *ChemPlusChem*, 2014, **79**, 375-381.
38. T. Chen, F. Deng, J. Zhu, C. Chen, G. Sun, S. Ma and X. Yang, *J. Mater. Chem.*, 2012, **22**, 15190-15197.
39. Q. Zhang, C. Li, Y. Chen, Z. Han, H. Wang, Z. Wang, D. Geng, W. Liu and Z. Zhang, *Appl. Phys. Lett.*, 2010, **97**, 133115.
40. T. Kasagi, T. Tsutaoka and K. Hatakeyama, *Appl. Phys. Lett.*, 2006, **88**, 172502.
41. P. F. Guan, X. F. Zhang and J. J. Guo, *Appl. Phys. Lett.*, 2012, **101**, 153108.
42. Y. Chen, P. Gao, C. Zhu, R. Wang, L. Wang, M. Cao and X. Fang, *J. Appl. Phys.*, 2009, **106**, 054303.
43. S. He, G.-S. Wang, C. Lu, J. Liu, B. Wen, H. Liu, L. Guo and M.-S. Cao, *J. Mater. Chem. A*, 2013, **1**, 4685-4692.
44. D. Chen, H. Quan, G. S. Wang and L. Guo, *ChemPlusChem*, 2013, **78**, 843-851.
45. P. H. Fang, *J. Chem. Phys.*, 1965, **42**, 3411-3413.
46. S. He, C. Lu, G.-S. Wang, J.-W. Wang, H.-Y. Guo and L. Guo, *ChemPlusChem*, 2014, **79**, 569-576.
47. M. Wu, Y. D. Zhang, S. Hui, T. D. Xiao, S. Ge, W. A. Hines, J. I. Budnick and G. W. Taylor, *Appl. Phys. Lett.*, 2002, **80**, 4404-4406.
48. S. Gangopadhyay, G. C. Hadjipanayis, B. Dale, C. M. Sorensen, K. J. Klabunde, V. Papaefthymiou and A. Kostikas, *Phys. Rev. B*, 1992, **45**, 9778-9787.
49. J. Guo, X. Wang, P. Miao, X. Liao, W. Zhang and B. Shi, *J. Mater. Chem.*, 2012, **22**, 11933-11942.
50. W. Li, T. Qiu, L. Wang, S. Ren, J. Zhang, L. He and X. Li, *ACS Appl. Mater. Interfaces*, 2012, **5**, 883-891.
51. W. Zhou, X. Hu, X. Bai, S. Zhou, C. Sun, J. Yan and P. Chen, *ACS Appl. Mater. Interfaces*, 2011, **3**, 3839-3845.
52. R. Li, T. Wang, G. Tan, W. Zuo, J. Wei, L. Qiao and F. Li, *J. Alloys Compd.*, 2014, **586**, 239-243.
53. C. Wang, X. Han, X. Zhang, S. Hu, T. Zhang, J. Wang, Y. Du, X. Wang and P. Xu, *J. Phys. Chem. C*, 2010, **114**, 14826-14830.
54. B. Gao, L. Qiao, J. Wang, Q. Liu, F. Li, J. Feng and D. Xue, *J. Phys. D: Appl. Phys.*, 2008, **41**, 235005.
55. F. Ma, J. Ma, J. Huang and J. Li, *J. Magn. Magn. Mater.*, 2012, **324**, 205-209.
56. Y. Cao, Q. Su, R. Che, G. Du and B. Xu, *Synth. Met.*, 2012, **162**, 968-973.
57. P. Xu, X. Han, C. Wang, D. Zhou, Z. Lv, A. Wen, X. Wang and B. Zhang, *J. Phys. Chem. B*, 2008, **112**, 10443-10448.
58. D. Micheli, C. Apollo, R. Pastore and M. Marchetti, *Compos. Sci. Technol.*, 2010, **70**, 400-409.
59. J. Shen, K. Chen, L. Li, W. Wang and Y. Jin, *J. Alloys Compd.*, 2014, **615**, 488-495.
60. B. Lu, H. Huang, X. L. Dong, X. F. Zhang, J. P. Lei, J. P. Sun and C. Dong, *J. Appl. Phys.*, 2008, **104**, 114313.